

# Surface Reconstruction Engineering with Synergistic Effect of Mixed-Salt Passivation Treatment toward Efficient and Stable Perovskite Solar Cells

Jiajia Suo, Bowen Yang,\* Edoardo Mosconi, Hyeon-Seo Choi, Yeonju Kim, Shaik M. Zakeeruddin, Filippo De Angelis, Michael Grätzel, Hui-Seon Kim,\* and Anders Hagfeldt\*

Surface passivation treatment is a widely used strategy to resolve trap-mediated nonradiative recombination toward high-efficiency metal-halide perovskite photovoltaics. However, a lack of passivation with mixture treatment has been investigated, as well as an in-depth understanding of its passivation mechanism. Here, a systematic study on a mixed-salt passivation strategy of formamidinium bromide (FABr) coupled with different F-substituted alkyl lengths of ammonium iodide is demonstrated. It is obtained better device performance with decreasing chain length of the F-substituted alkyl ammonium iodide in the presence of FABr. Moreover, they unraveled a synergistic passivation mechanism of the mixed-salt treatment through surface reconstruction engineering, where FABr dominates the reformation of the perovskite surface via reacting with the excess  $\text{PbI}_2$ . Meanwhile, ammonium iodide passivates the perovskite grain boundaries both on the surface and top perovskite bulk through penetration. This synergistic passivation engineering results in a high-quality perovskite surface with fewer defects and suppressed ion migration, leading to a champion efficiency of 23.5% with mixed-salt treatment. In addition, the introduction of the moisture resisted F-substituted groups presents a more hydrophobic perovskite surface, thus enabling the decorated devices with excellent long-term stability under a high humid atmosphere as well as operational conditions.


## 1. Introduction

Within only few years of development, solar-to-electrical power conversion efficiency (PCE) of perovskite solar cells (PSCs) has dramatically increased from 3.8% up to 25.5%.<sup>[1–7]</sup> Various defects readily generated at the grains and grain boundaries of the perovskite absorber layer as well as its corresponding interface are the main parameter which induces or accelerates a degradation of the perovskite layer, therefore being detrimental to device performance and inhibited from approaching to its theoretical limit.<sup>[8–10]</sup> Passivation treatment, however, as one of the most developed and effective strategies, can help to improve both efficiency and stability of the PSCs by suppressing recombination,<sup>[11,12]</sup> improving carrier extraction,<sup>[13,14]</sup> affecting energy band alignment, and/or physically separating selective contacts from the adjacent perovskite layer.<sup>[15,16]</sup>

So far, tremendous molecules have been developed as passivation materials

Dr. J. Suo, Dr. B. Yang, Y. Kim, Prof. A. Hagfeldt  
Laboratory of Photomolecular Science (LSPM)  
Institute of Chemical Sciences and Engineering  
School of Basic Sciences  
Ecole Polytechnique Fédérale de Lausanne  
Lausanne CH-1015, Switzerland  
E-mail: bowen.yang@epfl.ch; anders.hagfeldt@uu.se

Dr. E. Mosconi, Prof. F. De Angelis  
Computational Laboratory for Hybrid/Organic Photovoltaics (CLHYO)  
Istituto CNR di Scienze e Tecnologie Chimiche  
“Giulio Natta” (CNR-SCITEC)  
Perugia 06123, Italy

 The ORCID identification number(s) for the author(s) of this article can be found under <https://doi.org/10.1002/adfm.202102902>.

© 2021 The Authors. Advanced Functional Materials published by Wiley-VCH GmbH. This is an open access article under the terms of the Creative Commons Attribution License, which permits use, distribution and reproduction in any medium, provided the original work is properly cited.

DOI: 10.1002/adfm.202102902

H.-S. Choi, Prof. H.-S. Kim  
Department of Chemistry and Chemical Engineering  
Inha University  
Incheon 22212, Korea  
E-mail: hui-seon.kim@inha.ac.kr

Dr. S. M. Zakeeruddin, Prof. M. Grätzel  
Laboratory of Photonics and Interfaces (LPI)  
Institute of Chemical Sciences and Engineering  
School of Basic Sciences  
Ecole Polytechnique Fédérale de Lausanne  
Lausanne CH-1015, Switzerland

Prof. F. De Angelis  
Department of Chemistry  
Biology and Biotechnology  
University of Perugia  
Perugia 06123, Italy

Prof. A. Hagfeldt  
Department of Chemistry – Ångström Laboratory  
Uppsala University  
Box 523, Uppsala SE-75120, Sweden

being utilized as either additives in the perovskite precursor solutions or interlayers at the interfaces.<sup>[11,17,18]</sup> Among those, some of main components in perovskite precursors, such as methylammonium halide (MAX),<sup>[19,20]</sup> formamidinium halide (FAX),<sup>[21]</sup> and lead iodide (PbI<sub>2</sub>),<sup>[22–26]</sup> are commonly used as effective passivation materials and thus have been investigated from the perspective of performance enhancement of PSCs, where the inferior phase stability of the perovskite layer is still observed especially under humid atmosphere and illumination.<sup>[25]</sup> Ammonium halides with long alkyl or phenyl chain, on the other hand, have become popular candidates as passivation materials by either passivating the grain boundaries of the perovskites or forming an additional capping layer of low-dimensional perovskite at the interface to enhance photovoltaic performance and device stability.<sup>[12,27–32]</sup> For example, Kim and co-workers reported a systematic study on interfacial engineering on device performance and stability with different lengths of alkylammonium halide, butylammonium iodide (BAI), octylammonium iodide (OAI), and dodecylammonium iodide (DAI), achieving a certified efficiency of 22.9% with OAI treatment.<sup>[27]</sup> Jiang and co-workers applied phenethylammonium iodide (PEAI) post-treatment on the perovskite surface, which effectively reduced the surface defects and inhibited non-radiative recombination, resulting in a certified efficiency of 23.32%.<sup>[28]</sup> Similarly, pentafluoro-phenylethylammonium iodide (FEAI)<sup>[29]</sup> and 4-*tert*-butyl-benzylammonium iodide (tBBAI)<sup>[30]</sup> have been developed for further improvement in long-term stability, especially under a highly humid atmosphere. In addition, many other kinds of passivation materials have also been reported with excellent photovoltaic performance and superior stability, such as organic molecules, polymers, ionic liquids, and Lewis acids and bases.<sup>[33–44]</sup>

However, it needs great efforts to design such molecules which can achieve high efficiency in photovoltaic performance meanwhile present outstanding stability under different aging conditions. Mixed-salt passivation strategy proposed in this study, on the other hand, provides another way of designing functional passivation materials which get benefits from each individual passivation material as well as an additional synergistic effect from its combination. The role of F-substituted alkyl length of ammonium iodide is particularly explored in terms of surface passivation and energy alignment at the interface, which further help the design of passivation molecule without tremendous efforts for randomly employing various molecules as the passivation material. To our best knowledge, the majority of passivation materials developed so far are based on single molecule treatment. There are only few literatures introduced mixed-salt passivation strategy, however, without mentioning its synergistic passivation mechanism.<sup>[45,46]</sup> Thereby, in this paper, a systematic study on a mixed-salt passivation strategy of formamidinium bromide (FABr) coupled with different F-substituted alkyl lengths of ammonium iodides has been investigated on device performance and long-term stability.

## 2. Results and Discussion

The composition with mixed-cations and -halides (Cs<sub>0.05</sub>MA<sub>0.1</sub>FA<sub>0.85</sub>PbI<sub>2.9</sub>Br<sub>0.1</sub>·0.05PbI<sub>2</sub>), was chosen for the 3D

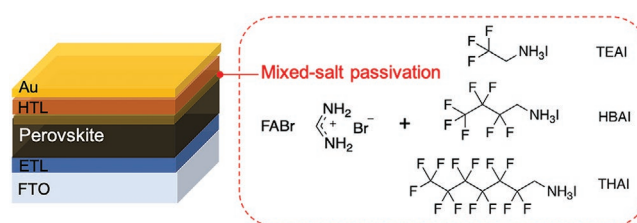


**Figure 1.** Device architecture (left) and molecular structure of FABr and the F-substituted alkyl ammonium iodide (TEAI, HBAI, and THAI). ETL and HTL denote electron transport layer and hole transport layer, respectively.

perovskite film to ensure its superior performance as well as the phase stability.<sup>[46]</sup> The 3D perovskite film was deposited on the substrate of fluorine-doped tin oxide (FTO)/compact (cp-) TiO<sub>2</sub>/mesoporous (mp-) TiO<sub>2</sub> by anti-solvent engineering process. Formamidinium bromide (FABr) was chosen to couple with different length of F-substituted alkyl ammonium iodide, CF<sub>3</sub>CH<sub>2</sub>NH<sub>3</sub>I (TEAI), CF<sub>3</sub>(CF<sub>2</sub>)<sub>2</sub>CH<sub>2</sub>NH<sub>3</sub>I (HBAI), and CF<sub>3</sub>(CF<sub>2</sub>)<sub>5</sub>CH<sub>2</sub>NH<sub>3</sub>I (THAI) (as shown in Figure 1), to form a mixed-salt passivation layer, denoting as TEAI·FABr, HBAI·FABr, and THAI·FABr, respectively. Post-treatment of the as-prepared perovskite layer was performed by spin-coating the solution containing the mixed-salt, which was followed by a post-annealing.

Current–voltage (*I*–*V*) characteristics of full devices with n-i-p architecture of FTO/cp-TiO<sub>2</sub>/mp-TiO<sub>2</sub>/perovskite/passivation layer (TEAI·FABr, HBAI·FABr, or THAI·FABr)/2,2',7,7'-tetrakis-(*N,N*-di-4-methoxyphenylamino)-9,9'-spirobifluorene (spiro-MeOTAD)/Au (shown in Figure 1) were measured. The statistical box charts of the photovoltaic parameters are shown in Figure 2a–d. The corresponding champion performance and average values are summarized in Table 1 and Table S1, Supporting Information, respectively. All three mixture passivation materials with different chain lengths of F-substituted alkyl ammonium iodides (TEAI·FABr, HBAI·FABr, and THAI·FABr) reveal negligible difference in photocurrent density (*J*<sub>SC</sub>), compared to the control devices without passivation, which is in accordance with the similar IPCE spectra and integrated *J*<sub>SC</sub> shown in Figure S1, Supporting Information. On the other hand, open-circuit voltage (*V*<sub>OC</sub>) and fill factor (FF) are significantly enhanced with a passivation layer of TEAI·FABr, HBAI·FABr, or THAI·FABr, leading to a dramatic increase in their PCEs.

A remarkable champion performance is achieved with the mixed-salt passivation by TEAI·FABr, showing a *J*<sub>SC</sub> of 24.96 mA cm<sup>-2</sup>, *V*<sub>OC</sub> of 1.161 V, FF of 0.813, and PCE of 23.50% (Figure 2e), with a stabilized power output of 23.23% at maximum power point (mpp) tracking, whereas the control device presents an undesirable decay within several minutes (Figure 2f). Interestingly, a post-treatment of perovskite film has been frequently reported mostly with long-alkylammonium halide which can effectively passivate the defect on perovskite surface and thus improve the device performance.<sup>[27,31]</sup> However, the opposite phenomena has been observed in this study, where better device performance is obtained as decreasing the chain length of the F-substituted alkyl ammonium iodide in the presence of FABr. It is highly proposed that the ammonium

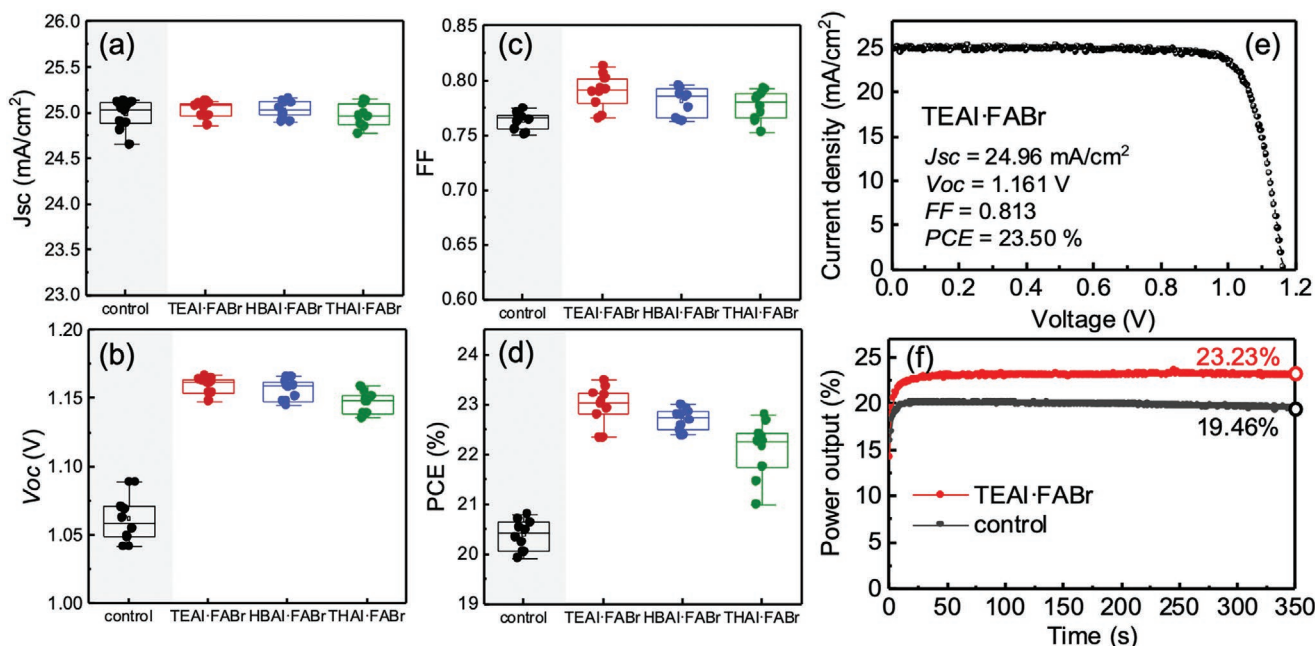


**Figure 2.** Statistical box charts for the photovoltaic parameters of a)  $J_{sc}$ , b)  $V_{oc}$ , c) FF, and d) PCE of devices without passivation layer (control, black) and with passivation layers of mixed-salt: TEAI·FABr (red), HBAI·FABr (blue), and THAI·FABr (green). e)  $I-V$  curve of the champion device with TEAI·FABr passivation treatment. f) Power output of the device without (black) and with TEAI·FABr passivation treatment (red) at maximum power point as a function of time.

iodides with different chain lengths play a different role in passivating the perovskite film while mixing with FABr. Therefore, a systematic investigation is carried out to elucidate its passivation mechanism in this study.

In order to reveal the effect on perovskite surface morphology of post-treatment with the mixed-salt passivation materials, scanning electron microscopies (SEM) were carried out and are shown in **Figure 3a–d**. The white flakes, presented in the pristine 3D perovskite film (**Figure 3a**) are indicative of  $PbI_2$ ,<sup>[24]</sup> which readily disappears after the post-treatment (**Figure 3b–d**). This implies a reaction between the excessive  $PbI_2$  from the underlying 3D perovskite and the passivation salts (TEAI·FABr, HBAI·FABr, or THAI·FABr) on surface during the post-annealing process, which compensates the inferior film morphology with smaller grain size and presence of pinholes created by the unreacted  $PbI_2$ ,<sup>[22]</sup> resulting in an improved perovskite surface with more uniformity and homogeneity compare to the pristine perovskite film. The overall increase in the grain size after the post-annealing process with mixed passivation salts is consistently observed as shown in **Figure S2**, Supporting Information, where the average grain size of the control, TEAI·FABr-, HBAI·FABr-, and THAI·FABr-treated films is 154,

216, 227, and 252 nm, respectively. The improved crystal quality by the mixed salts is also evident with grazing incidence X-ray diffraction (GIXRD) patterns which delivers the crystal information on the perovskite surface (**Figure 3e**). The  $PbI_2$  peak at  $12.6^\circ$  shown in the control sample is effectively removed by the post-treatment with the mixed-salt of TEAI·FABr, HBAI·FABr, or THAI·FABr. Moreover, the grain size is apparently increased by the post-treatment with the mixed salts while the surface morphology is mostly retained by passivating the perovskite film with individual salts of TEAI, HBAI, or THAI in the absence of FABr, showing a remaining  $PbI_2$  (**Figures S3 and S4**, Supporting Information). The notable changes in surface morphology are found to selectively occur only in the presence of FABr, indicating that the reaction is governed by FABr through the formation of an ultra-thin layer of  $FAPbI_xBr_{3-x}$ . Therefore, the increased grain size by the mixed-salt passivation underlies that the alkyl ammonium iodide (TEAI, HBAI, or THAI) is also involved in the surface crystal reconstruction, while coupling with FABr. On the other hand, negligible change is observed from the cross-sectional SEM images regardless of the post-treatment with mixed-salts (**Figure S5**, Supporting Information) which accounts for the surface-limited crystal reconstruction.

**Table 1.** Champion photovoltaic parameters of PSCs without and with mixed-salt passivation of TEAI·FABr, HBAI·FABr, and THAI·FABr, respectively.

Salt composition for the passivation layer	$J_{sc}$ [mA cm <sup>-2</sup> ]	$V_{oc}$ [V]	FF	PCE [%]
Control	25.05	1.073	0.77	20.65
TEAI·FABr	24.96	1.161	0.81	23.50
HBAI·FABr	25.02	1.159	0.80	23.02
THAI·FABr	25.09	1.148	0.80	22.81

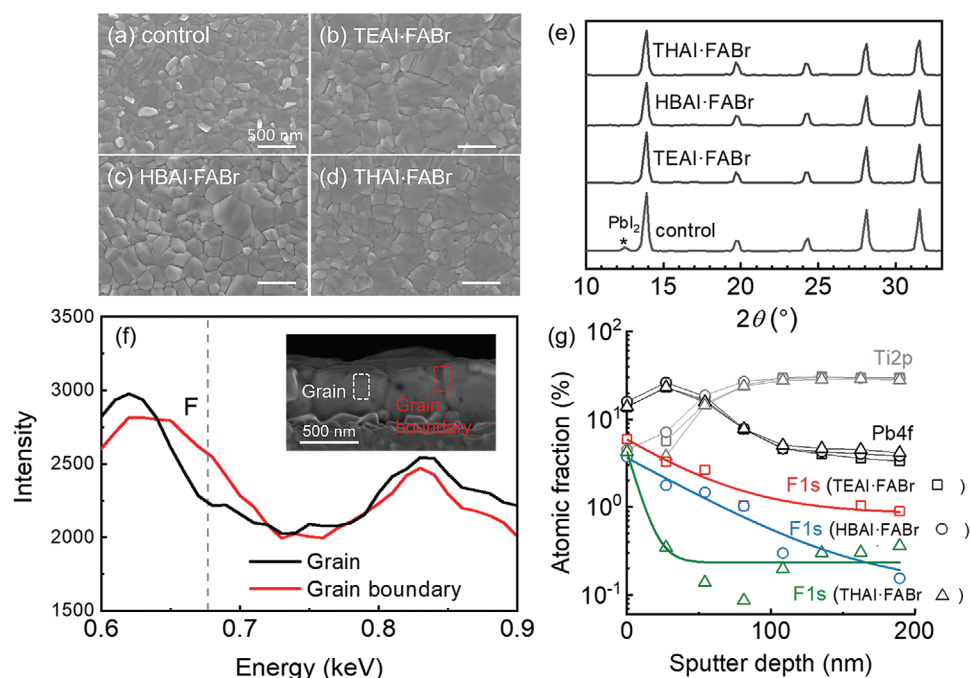


**Figure 3.** Surface HR-SEM images of perovskite films a) without and with different mixed-salt passivation treatment of b) TEAI·FABr, c) HBAI·FABr, and d) THAI·FABr. e) GIXRD patterns of control, perovskite film passivated with TEAI·FABr, HBAI·FABr, and THAI·FABr. f) EDS spectra measured on the grain and grain boundary of the TEAI·FABr passivated perovskite film. Insert figure shows the corresponding cross-section SEM image of the film for element analysis of grain and grain boundary. g) XPS depth profiling of the mixed-salt passivated films with TEAI·FABr, HBAI·FABr, and THAI·FABr.

To further disclose the mixed-salt passivation mechanism, element analysis of the perovskite film post-treated by TEAI·FABr, demonstrating the best performance was investigated using energy dispersive X-ray spectroscopy (EDS). As shown in Figure 3f (full spectrum is shown in Figure S6, Supporting Information), the fluorine atom from TEAI is dominantly monitored from the grain boundaries rather than grains, suggesting that the F-substituted alkyl ammonium iodide is expected to not only passivate the perovskite surface, but also diffuse longitudinally along the grain boundary. Furthermore, X-ray photoelectron spectroscopy (XPS) depth profiling was measured to investigate the effect of different lengths of TEAI, HBAI, and THAI on the diffusion depth along the grain boundary, indicated in Figure 3g. It is noted that the shorter length the alkyl ammonium iodide employs, the deeper the molecule diffuses into the underlying 3D perovskite bulk film. In other words, TEAI with the shortest chain length can more effectively passivate the surface of 3D perovskite layer by reaching a deeper depth from the top surface through the grain boundary, whereas THAI, with the longest alkyl chain, is mainly distributed on the 3D perovskite surface.

The effect of mixed-salt on the work function at the perovskite surface was investigated by Kelvin probe force microscopy (KPFM). Contact potential difference ( $V_{CPD}$ ) between sample and tip was monitored in the dark to calculate the work function of the sample ( $\Phi_{\text{sample}}$ ) according to Equation (1) by calibrating with highly oriented pyrolytic graphite (HOPG).<sup>[47]</sup>

$$\Phi_{\text{sample}} = 4.65 + V_{CPD}(\text{HOPG}) - V_{CPD}(\text{sample}) \quad (1)$$

Table 2 represents  $V_{CPD}$  of the perovskite film with post-treatment depending on the mixed-salt as well as only FABr for passivation and correspondingly estimated work function. The passivated films with either FABr or mixed-salts (TEAI·FABr, HBAI·FABr, and THAI·FABr) resulted in higher  $V_{CPD}$  values compared to that of the control sample without any post-treatment. A trap-rich perovskite film shows a relatively lower  $V_{CPD}$ ,<sup>[48]</sup> while the  $V_{CPD}$  is increased as ions of salts effectively compensate the vacancy defects.<sup>[49,50]</sup> Therefore, the increased  $V_{CPD}$  is ascribed to the reduced trap density of the control sample by surface passivation through mixed-salt treatment, which is particularly pronounced with TEAI·FABr and HBAI·FABr, implying the effective passivation effect of the mixed salts. Furthermore, 5.11 eV of the estimated work function of the control sample, in consistency with reported values,<sup>[51]</sup> is shifted upward by applying the mixed-salt treatment, leading to a change in band alignment on the surface. The upshifted work function on the surface suggests more p-type character near the spiro-MeOTAD; being beneficial

**Table 2.** Contact potential difference ( $V_{CPD}$ ) and estimated work function of perovskite surface depending on the passivation materials.

Salt composition for the passivation layer	$V_{CPD}$ [mV]	Work function [eV]
Control	102.447	5.11
FABr	210.122	5.02
TEAI·FABr	237.380	4.99
HBAI·FABr	249.181	4.98
THAI·FABr	193.518	5.04

for the hole extraction. When considering the work function of spiro-MeOTAD of 4.90 eV, the graded energy alignment between perovskite and spiro-MeOTAD indeed enables photogenerated holes to be effectively collected.<sup>[51]</sup> Therefore, TEAI·FABr and HBAI·FABr would not only successfully passivate the surface defects by the crystal reconstruction on surface but also build a beneficial energy alignment between perovskite and spiro-MeOTAD, being responsible for the greatly enhanced photovoltaic properties.

As evidenced from the discussion above, here, we propose a synergistic effect of the mixed salts (FABr and F-substituted alkyl ammonium iodide) on passivating the perovskite film. The mixture of TEAI·FABr was selected for further analysis based on its best performance among the mixed salts. Therefore, we fabricated photovoltaic devices without and with passivation treatment of individual salts (TEAI or FABr) and the mixture of TEAI·FABr. The corresponding statistical box charts of the photovoltaic parameters and the champion performance are summarized in Figure S7, Supporting Information, and Table 3. Devices with individual passivation treatment by TEAI or FABr resulted in enhanced PCE, however, dramatic improvement is observed by the mixed-salt passivation treatment with TEAI·FABr, with the increment of both  $V_{OC}$  and FF. The more concentration dependence on the mixed-salt of TEAI<sub>x</sub>·FABr<sub>1-x</sub> was evaluated by varying the ratio of TEAI ( $X = 0, 0.25, 0.5, 0.75, \text{ and } 1.00$ ) while remaining at the same total molarity, as shown in Table S2, Supporting Information, which proves the most optimized ratio of  $X = 0.5$  between TEAI and FABr. Concurrently, a drastic decrease in hysteresis index (HI), illustrated in Table 3, is obtained from the devices passivated by both TEAI and the mixed-salt of TEAI·FABr, compared to the ones without TEAI (control and FABr treated devices). The stabilized PCEs can be assumed in Figure S8, Supporting Information, where the time-dependent power output is shown depending on the passivation salt. Combined with EDS and XPS depth profiling results, the elimination of hysteresis in the TEAI involved PSCs could attribute to the reduced Frenkel defects and inhibited ion migration of iodide vacancy by introducing excess iodide from TEAI.<sup>[42]</sup> These excess halides can thereby passivate the non-radiative recombination pathways on the perovskite surface. Remarkably, as indicated above, while post-annealing the mixed-salt of TEAI·FABr, TEAI not only contributes to the

crystal reformation of the FAPbI<sub>x</sub>Br<sub>3-x</sub> on surface but also penetrates into the top of the 3D perovskite bulk.

Moreover, as shown in Figure 4, <sup>1</sup>H NMR (<sup>1</sup>H nuclear magnetic resonance) measurements were carried out to analyze the interaction between FABr and TEAI. The active proton chemical peak of FABr amino groups (8.90 ppm) is split into three peaks (9.02, 8.72, and 8.68 ppm) in the mixture solution of TEAI·FABr, combined with the <sup>1</sup>H-<sup>1</sup>H COSY spectroscopy (Figures 4a and 4b). Except for the anion effect, the similar split is also observed in the mixed-salt of TEAI·FAI compared with the <sup>1</sup>H NMR spectrum of FAI solution (Figures 4c and 4d). These movements of chemical shift correspond to changes of hydrogen nucleus electron cloud density which are caused by strong H–F hydrogen bonding between FA<sup>+</sup> and TEA<sup>+</sup>. Except for the <sup>1</sup>H NMR spectra, the strong interaction between H–F was also observed from the <sup>19</sup>F NMR spectra, as shown in Figure S9, Supporting Information. Compared to the <sup>19</sup>F peaks of TEAI, the downfield shift movement with altered coupling interaction was observed in the mixed-salt solution, which is caused by the H–F hydrogen bonding between FA<sup>+</sup> cation and TEA<sup>+</sup> cation. Therefore, it is confirmed that a strong internal interaction between FABr and TEAI plays an important role in the perovskite crystal reconstruction during the post-treatment, leading to an enhanced quality of the perovskite surface. Also, this internal interaction effectively enables us to restrain ions from moving, which suppresses halide migration and inhibits additional non-radiative recombination arising from interstitial halides.<sup>[53]</sup> This is also consistent with the reduced *I*–*V* hysteresis of the TEAI involved passivation treatment, shown in Table 3.

To gain insight into the nature of the interaction between the TEAI and FABr on the perovskite surface, we simulated the interface following the approach reported previously<sup>[46]</sup> and detailed in the Supporting Information. We mainly focused the attention on the evaluation of role of the hydrogen bond and the electrostatic interaction between the FA<sup>+</sup> and the fluorine atoms of the TEAI salt. In particular, we performed density functional theory (DFT) calculation of a MAPbI<sub>3</sub> perovskite surface fully covered by TEAI·FABr. A PbI<sub>2</sub>-rich perovskite surface was set as a control. One layer of FABr was added on top, where the Br species are bonded to the undercoordinated Pb atoms. Another layer of TEAI layer was subsequently added

**Table 3.** Photovoltaic parameters and hysteresis index (HI) of champion PSCs without passivation layer and with passivation layers by TEAI, FABr, and mixed-salt of TEAI·FABr.

Salt composition for the passivation layer	$J_{sc}$ [mA cm <sup>-2</sup> ]	$V_{oc}$ [V]	FF	PCE [%]	HI <sup>c)</sup> [%]
Control-RS <sup>a)</sup>	25.05	1.073	0.77	20.65	6.6
Control-FS <sup>b)</sup>	25.03	1.052	0.73	19.28	
TEAI-RS	24.89	1.128	0.78	21.56	1.5
TEAI-FS	25.04	1.116	0.76	21.23	
FABr-RS	24.92	1.156	0.79	22.88	3.6
FABr-FS	24.97	1.142	0.78	22.04	
TEAI·FABr-RS	24.96	1.161	0.81	23.50	1.0
TEAI·FABr-FS	25.03	1.160	0.80	23.25	

<sup>a)</sup>Reverse scan; <sup>b)</sup>Forward scan; <sup>c)</sup>HI =  $(PCE_{RS} - PCE_{FS})/PCE_{RS}$ .

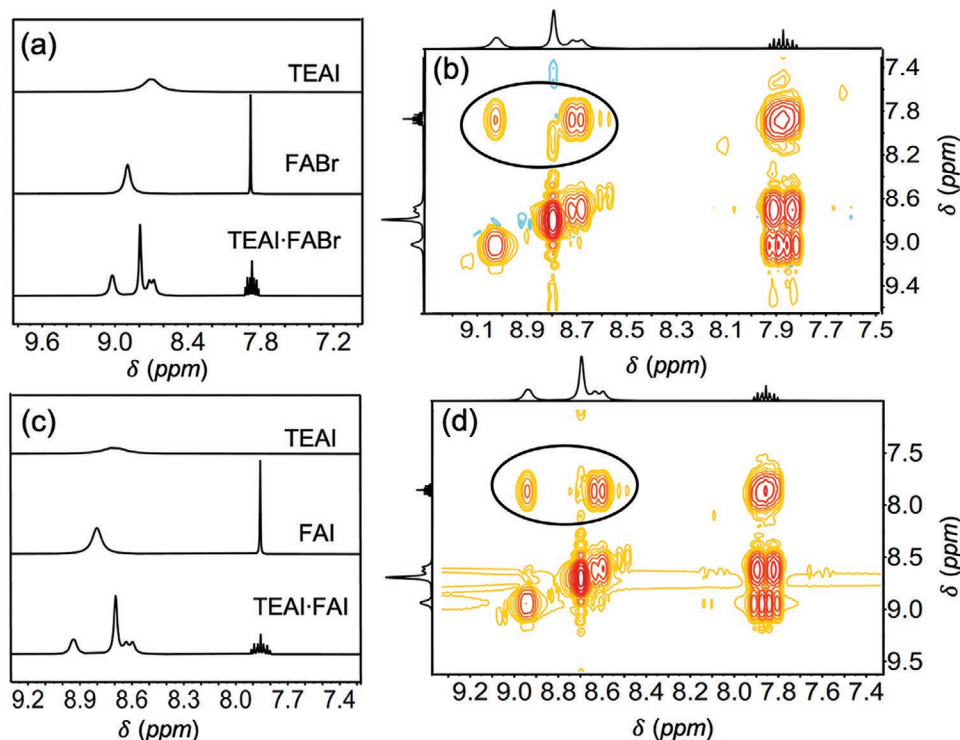


**Figure 4.** a)  $^1\text{H}$  NMR spectra of TEAI, FABr, and mixed-salt of TEAI·FABr (molar ratio = 1:1) in DMSO-d<sub>6</sub>. b)  $^1\text{H}$ - $^1\text{H}$  COSY spectrum of mixed-salt of TEAI·FABr (molar ratio = 1:1) in DMSO-d<sub>6</sub>. c)  $^1\text{H}$  NMR spectra of TEAI, FAI, and mixed-salt of TEAI·FAI (molar ratio = 1:1) in DMSO-d<sub>6</sub>. d)  $^1\text{H}$ - $^1\text{H}$  COSY spectrum of mixed-salt of TEAI·FAI (molar ratio = 1:1) in DMSO-d<sub>6</sub>.

on top of the perovskite-bound FABr layer. **Figure 5** shows the TEAI·FABr passivated surface along with the corresponding HBAI·FABr interface model.<sup>[46]</sup> The TEAI·FABr interaction is found to take place through the fluorine atoms in TEAI and the hydrogen atoms in FABr, which is in line with the results obtained from HBAI. To evaluate the stability of the covering layer, we calculated the interaction energy ( $E_{\text{int}}$ ) between the FABr and TEAI layers. This quantity is associated to adsorption of a salt overlayer ( $E_{\text{int}}$ ) and is calculated with reference to the isolated gas-phase molecules, see Supporting Information.

An  $E_{\text{int}}$  of 1.10 eV is obtained between TEAI and FABr layers, which is higher than that of the HBAI·FABr (0.96 eV) layer, indicating a more stable interface with TEAI·FABr, with respect to HBAI·FABr. This higher stability also suggests a more compact passivation layer generated by TEAI·FABr, which restrains the ions from moving on the surface, as already proposed. In particular, Zhang et al. reported that F atoms in FE polymers could make a strong interaction with  $\text{MA}^+$  or  $\text{FA}^+$  and that the resulting binding force could enable these ions to be restrained from moving.<sup>[53]</sup> By considering this aspect, the higher  $E_{\text{int}}$

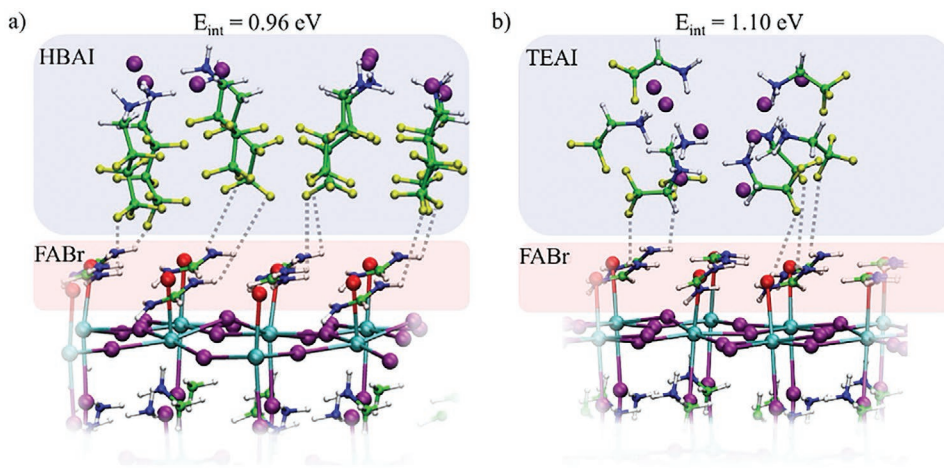


**Figure 5.** a) HBAI-FABr-passivated perovskite interface. b) TEAI-FABr-passivated perovskite interface.

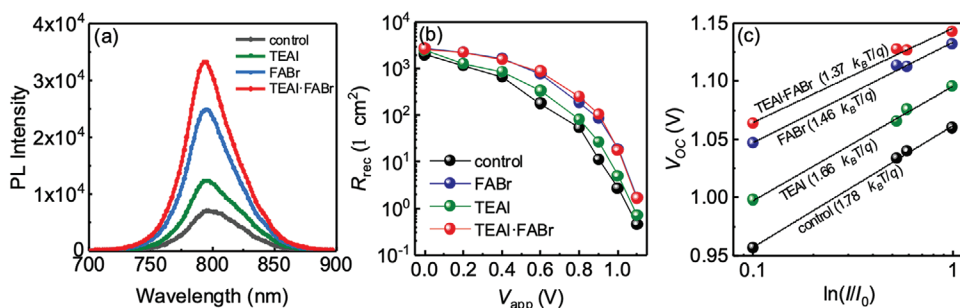


**Figure 6.** a) Steady-state PL spectra of pristine perovskite film (control), perovskite films treated with TEAI, FABr, and mixed-salt of TEAI-FABr. b) Recombination resistance. c)  $V_{oc}$  as a function of light intensity on devices without (control) and with passivation treatments of TEAI, FABr, and TEAI-FABr.

calculated for TEAI could be associated to a higher tendency of TEAI to reduce ions mobility on the surface with respect to HBAI. Nevertheless, the electronic property of the mixture passivation layer with TEAI-FABr shows a similar effect compared to HBAI-FABr in reducing the surface traps associated to the under-coordinated lead atoms of the  $PbI_2$ -rich surface, shown in Figure S10, Supporting Information.

In order to further evaluate this synergistic effect, surface traps were studied by performing steady-state photoluminescence (PL) of the samples with and without the post-treatment with individual passivation of TEAI or FABr, and mixture passivation of >TEAI-FABr, respectively. Steady-state PL spectra present higher peak intensities with all post-treatments compared to the control film (Figure 6a). The highest PL peak is notably obtained from the treatment with TEAI-FABr, indicating the most pronounced effect on suppressing the surface recombination as indicated by the theoretical analysis. Figure 6b shows the recombination resistance ( $R_{rec}$ ) of devices depending on the individual passivation of TEAI or FABr, and mixture passivation of TEAI-FABr.  $R_{rec}$ s are comparable at short-circuit condition, being responsible for the observed similar  $J_{SC}$ , while the difference is pronounced with applying the bias voltage toward open-circuit voltage, leading to a difference in FF and  $V_{oc}$ . The control device results in the lowest  $R_{rec}$  across the whole bias voltage range, although  $R_{rec}$  is slightly increased by employing TEAI. Whereas, the post-treatment of FABr apparently improves  $R_{rec}$ , showing the increment by one order at 0.9 V. The improvement is further slightly increased by employing the mixed-salt of TEAI-FABr, particularly between 0.6 and 0.9 V, being responsible for slightly higher FF with similar  $V_{oc}$  from the device based on TEAI-FABr treatment compared to the device with FABr. The recombination behavior is greatly supported by the ideality factor of the devices which are obtained by measuring the  $V_{oc}$  response under a different light intensity, as shown in Figure 6c. The control device shows a slope of  $1.78 k_B T/q$  (where  $k_B$  is the Boltzmann constant,  $T$  is temperature, and  $q$  is the electric charge), while the mixed-salt passivation with TEAI-FABr shows the smallest slope ( $1.37 k_B T/q$ ), compared with either individual passivation material (FABr or TEAI). The reduced ideality factor closes to 1 confirms that the trap-assisted Shockley-Read-Hall recombination is significantly suppressed by the surface reconstruction based on the TEAI-FABr post-treatment.<sup>[54,55]</sup>

Additionally, in order to reveal the synergistic effect on the stability of the perovskite film and device, we measured the

contact angle of water droplets on the pristine perovskite (control) and passivated films with FABr, TEAI, and TEAI-FABr as shown in Figure 7a–d, respectively. It is suggested that the passivated surface by FABr is highly sensitive to the moisture though its passivating effect is prominent as discussed above. However, through coupling with more moisture resistive F-substituted alkyl ammonium iodide, the passivated surface becomes more robust to moisture and would correspondingly lead to a better humid stability. Accordingly, we exposed the nonencapsulated PSC devices without and with TEAI-FABr treatment under high R.H. of  $\approx 30$ –60% in dark for 800 h. While the normalized PCE drops by 20% from its initial performance without passivation layer, the mixed-salt modified device notably remains a remarkable 98% of its initial PCE. It is worth noticing that the devices treated with the other two mixed-salt passivation of HBAI-FABr and THAI-FABr also present outstanding stabilities of negligible PCE drops owing to its excellent hydrophobicity induced by the F atoms in the ammonium cations, as shown in Figure S11, Supporting Information.

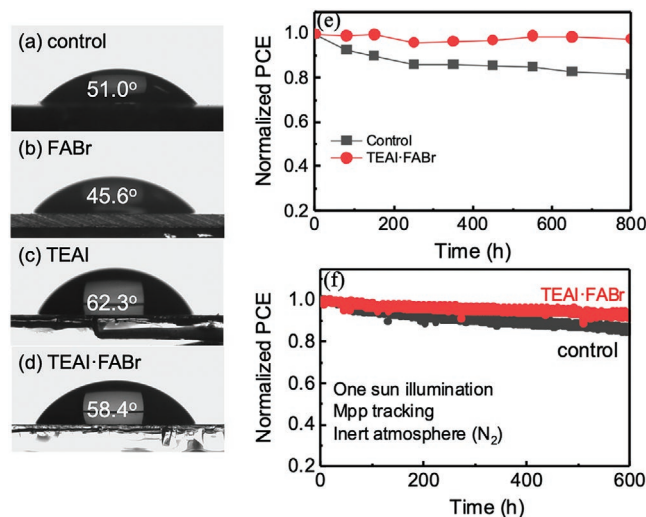


**Figure 7.** Contact angle of water droplet on perovskite surfaces a) without and with passivation layers of b) FABr, c) TEAI, and d) TEAI-FABr. e) Long-term stability of control device (black) and with TEAI-FABr treated device (red) under dark with relative humidity (R.H.) of 30% to 60%. f) Stability of normalized PCEs of non-encapsulated control device (black) and with TEAI-FABr treated device (red) under (a) maximum power point (mpp) tracking with one sun illumination in  $N_2$  atmosphere.

However, in sharp contrast, the PSC device passivated with only FABr shows a severe decay under the same aging conditions, with a PCE loss of about 20%, even worse than the control device, indicating that although FABr passivation proves a great enhancement in device performance as discussed above, it is sensitive in high humid atmosphere. However, such a problem can be solved by introducing TEAI, HBAI, or THAI, simultaneously, which can not only further passivate the perovskite surface, but also enhance the stability of the device, especially under high humidity. In addition, we also monitored the operational stability of devices without and with TEAI·FABr treatment, aging at room temperature for 600 h of continuous full sun illumination at mpp tracking in a nitrogen atmosphere, illustrated in Figure 7f. The control device loses 15% of their initial PCE, while the device with TEAI·FABr treatment retains more than 92%. Overall, the observed stability results highlight the importance of the synergistic effect of the mixed-salt passivation strategy on PSCs from the long-term point of view.

### 3. Conclusion

In summary, we, for the first time, have developed the role of a mixed-salt passivation strategy of FABr coupled with different F-substituted alkyl lengths of ammonium iodide (TEAI, HBAI, or THAI) in improving optoelectronic properties and long-term stability of PSCs. A better device performance was obtained as decreasing the chain length of the F-substituted alkyl ammonium iodide in the presence of FABr via a passivation mechanism with synergistic effect through surface reconstruction engineering has been proposed. Our mixed-salt passivation strategy enabled us to demonstrate n-i-p structured devices with efficiencies over 23% and outstanding long-term stability under operational condition as well as shelf condition with a highly humid atmosphere. More generally, our findings provide more possibilities and an essential path on designing more effective passivation materials in the future of photovoltaic devices in order to achieve highly efficient devices with a simultaneously outstanding long-term stability.

### Supporting Information

Supporting Information is available from the Wiley Online Library or from the author.

### Acknowledgements

This project has received funding from the European Union's Horizon 2020 research and innovation program under grant agreement No 764047 and from the Swiss National Science Foundation for financial support with Project No. 200020\_185041. This work was supported by the National Research Foundation of Korea (NRF) grant funded by the Korea government (MSIT) (No. 2021R1C1C1009686).

### Conflict of Interest

The authors declare no conflict of interest.

### Author Contributions

J.S. and B.Y. contributed equally to this work. J.S. and B.Y. conceived the idea, prepared films, and fabricated all devices and characterizations. M.E. and A.D.F. carried out DFT calculation and analysis. H.-S.K. and H.-S.C. assisted in KPFM measurements and IS analysis. Y.K. performed steady-state PL measurements. J.S., B.Y., and H.-S.K. analyzed all data and wrote the manuscript. A.H. directed the overall research. All authors read and commented on the manuscript.

### Data Availability Statement

The data that supports the findings of this study are available in the supplementary material of this article. The data that support the findings of this study are available from the corresponding author upon reasonable request.

### Keywords

mixed-salt passivation, perovskite solar cells, surface reconstruction engineering, synergistic effects

Received: April 15, 2021

Revised: May 15, 2021

Published online: June 17, 2021

- [1] A. Kojima, K. Teshima, Y. Shirai, T. Miyasaka, *J. Am. Chem. Soc.* **2009**, *131*, 6050.
- [2] H.-S. Kim, C.-R. Lee, J.-H. Im, K.-B. Lee, T. Moehl, A. Marchioro, S.-J. Moon, R. Humphry-Baker, J.-H. Yum, J. E. Moser, M. Grätzel, N.-G. Park, *Sci. Rep.* **2012**, *2*, 591.
- [3] M. M. Lee, J. Teuscher, T. Miyasaka, T. N. Murakami, H. J. Sanith, *Science* **2012**, *338*, 643.
- [4] K. Wang, D. Yang, C. Wu, M. Sanghadasa, S. Priya, *Prog. Mater. Sci.* **2019**, *106*, 100580.
- [5] H.-S. Kim, A. Hagfeldt, N.-G. Park, *Chem. Commun.* **2019**, *55*, 1192.
- [6] W. Du, S. Zhang, Q. Zhang, X. Liu, *Adv. Mater.* **2019**, *31*, 1804894.
- [7] Best Research-Cell Efficiencies Chart, <https://www.nrel.gov/pv/assets/pdfs/best-research-cell-efficiencies.20210207.pdf> (accessed: February 2021).
- [8] J. Chen, N.-G. Park, *Adv. Mater.* **2019**, *31*, 1803019.
- [9] D. Luo, R. Su, W. Zhang, Q. Gong, R. Zhu, *Nat. Rev. Mater.* **2020**, *5*, 44.
- [10] C. M. Wolff, P. Caprioglio, M. Stolterfoht, D. Neher, *Adv. Mater.* **2019**, *31*, 1902762.
- [11] F. Gao, Y. Zhao, X. Zhang, J. You, *Adv. Energy Mater.* **2020**, *10*, 1902650.
- [12] S. Wu, J. Zhang, Z. Li, D. Liu, M. Qin, S. H. Cheung, X. Lu, D. Lei, S. K. So, Z. Zhu, A. K.-Y. Jen, *Joule* **2020**, *4*, 1248.
- [13] F. Wan, X. Qiu, H. Chen, Y. Liu, H. Xie, J. Shi, H. Huang, Y. Yuan, Y. Gao, C. Zhou, *Org. Electron.* **2018**, *59*, 184.
- [14] J. Y. Seo, R. Uchida, H. S. Kim, Y. Saygili, J. Luo, C. Moore, J. Kerrod, A. Wagstaff, M. Eklund, R. McIntyre, N. Pellet, S. M. Zakeeruddin, A. Hagfeldt, M. Grätzel, *Adv. Funct. Mater.* **2018**, *28*, 1705763.
- [15] P. Chen, X. Yin, M. Que, Y. Yang, W. Que, *RSC Adv.* **2016**, *6*, 57996.
- [16] X. Xu, H. Zhang, J. Shi, J. Dong, Y. Luo, D. Li, Q. Meng, *J. Mater. Chem. A* **2015**, *3*, 19288.
- [17] P. Zhao, B. J. Kim, H. S. Jung, *Mater. Today Energy* **2018**, *7*, 267.
- [18] R. Fan, W. Zhou, Z. Huang, H. Zhou, *EnergyChem* **2020**, *2*, 100032.
- [19] T. Zhang, M. Long, K. Yan, M. Qin, X. Lu, X. Zeng, C. M. Cheng, K. S. Wong, P. Liu, W. Xie, J. Xu, *Adv. Energy Mater.* **2017**, *7*, 1700118.

- [20] M. Mateen, Z. Arain, Y. Yang, X. Liu, S. Ma, C. Liu, Y. Ding, X. Ding, M. Cai, S. Dai, *ACS Appl. Mater. Interfaces* **2020**, *12*, 10535.
- [21] K. T. Cho, S. Paek, G. Grancini, C. Roldán-Carmona, P. Gao, Y. Lee, M. K. Nazeeruddin, *Energy Environ. Sci.* **2017**, *10*, 621.
- [22] T. J. Jacobsson, J.-P. Correa-Baena, E. H. Anaraki, B. Philippe, S. D. Stranks, M. E. F. Bouduban, W. Tress, K. Schenk, J. Teuscher, J.-E. Moser, H. Rensmo, A. Hagfeldt, *J. Am. Chem. Soc.* **2016**, *138*, 10331.
- [23] D. Bi, W. Tress, M. I. Dar, P. Gao, J. Luo, C. Renevier, K. Schenk, A. Abate, F. Giordano, J.-P. C. Baena, J.-D. Decoppet, S. M. Zakeeruddin, M. K. Nazeeruddin, M. Grätzel, A. Hagfeldt, *Sci. Adv.* **2016**, *2*, e1501170.
- [24] Q. Chen, H. Zhou, T.-B. Song, S. Luo, Z. Hong, H.-S. Duan, L. Dou, Y. Liu, Y. Yang, *Nano Lett.* **2014**, *14*, 4158.
- [25] F. Liu, Q. Dong, M. K. Wong, A. B. Djurišić, A. Ng, Z. Ren, Q. Shen, C. Surya, W. K. Chan, J. Wang, A. M. C. Ng, C. Liao, H. Li, K. Shih, C. Wei, H. Su, J. Dai, *Adv. Energy Mater.* **2016**, *6*, 1502206.
- [26] H. Wang, Z. Wang, Z. Yang, Y. Xu, Y. Ding, L. Tan, C. Yi, Z. Zhang, K. Meng, G. Chen, Y. Zhao, Y. Luo, X. Zhang, A. Hagfeldt, J. Luo, *Adv. Mater.* **2020**, *32*, 2000865.
- [27] H. Kim, S.-U. Lee, D. Y. Lee, M. J. Paik, H. Na, J. Lee, S. I. Seok, *Adv. Energy Mater.* **2019**, *9*, 1902740.
- [28] Q. Jiang, Y. Zhao, X. Zhang, X. Yang, Y. Chen, Z. Chu, Q. Ye, X. Li, Z. Yin, J. You, *Nat. Photonics* **2019**, *13*, 460.
- [29] Y. Liu, S. Akin, L. Pan, R. Uchida, N. Arora, J. Milić, A. Hinderhofer, F. Schreiber, A. R. Uhl, S. M. Zakeeruddin, A. Hagfeldt, M. I. Dar, M. Grätzel, *Sci. Adv.* **2019**, *5*, eaaw2543.
- [30] H. Zhu, Y. Liu, F. T. Eickemeyer, L. Pan, D. Ren, M. A. Ruiz-Preciado, B. Carlsen, B. Yang, X. Dong, Z. Wang, H. Liu, S. Wang, S. M. Zakeeruddin, A. Hagfeldt, M. I. Dar, X. Li, M. Grätzel, *Adv. Mater.* **2020**, *32*, 1907757.
- [31] J. J. Yoo, S. Wieghold, M. C. Sponseller, M. R. Chua, S. N. Bertram, N. T. P. Hartono, J. S. Tresback, E. C. Hansen, J.-P. Correa-Baena, V. Bulović, T. Buonassisi, S. S. Shin, M. D. Bawendi, *Energy Environ. Sci.* **2019**, *12*, 2192.
- [32] X. Zheng, Y. Hou, C. Bao, J. Yin, F. Yuan, Z. Huang, K. Song, J. Liu, J. Troughton, N. Gasparini, C. Zhou, Y. Lin, D. Xue, B. Chen, A. K. Johnston, N. Wei, M. N. Hedhili, M. Wei, A. Y. Alsalloum, P. Maity, B. Turedi, C. Yang, D. Baran, T. D. Anthopoulos, Y. Han, Z. Lu, O. F. Mohammed, F. Gao, E. H. Sargent, O. M. Bakr, *Nat. Energy* **2020**, *5*, 131.
- [33] R. Wang, J. Xue, K.-L. Wang, Z.-K. Wang, Y. Luo, D. Fenning, G. Xu, S. Nuryyeva, T. Huang, Y. Zhao, J. Y. Yang, J. Zhu, M. Wang, S. Tan, I. Yavuz, K. N. Houk, Y. Yang, *Science* **2019**, *366*, 1509.
- [34] Q. Hu, W. Chen, W. Yang, Y. Li, Y. Zhou, B. W. Larson, J. C. Johnson, Y. Lu, W. Zhong, J. Xu, L. Klivansky, C. Wang, M. Salmeron, A. B. Djurišić, F. Liu, Z. He, R. Zhu, T. P. Russell, *Joule* **2020**, *4*, 1575.
- [35] Y. Cai, J. Cui, M. Chen, M. Zhang, Y. Han, F. Qian, H. Zhao, S. Yang, Z. Yang, H. Bian, T. Wang, K. Guo, M. Cai, S. Dai, Z. Liu, S. Liu, *Adv. Funct. Mater.* **2021**, *31*, 2005776.
- [36] D. Bi, C. Yi, J. Luo, J.-D. Decoppet, F. Zhang, S. M. Zakeeruddin, X. Li, A. Hagfeldt, M. Grätzel, *Nat. Energy* **2016**, *1*, 16142.
- [37] M. Kim, S. G. Motti, R. Sorrentino, A. Petrozza, *Energy Environ. Sci.* **2018**, *11*, 2609.
- [38] T. Niu, J. Lu, R. Munir, J. Li, D. Barrit, X. Zhang, H. Hu, Z. Yang, A. Amassian, K. Zhao, S. F. Liu, *Adv. Mater.* **2018**, *30*, 1706576.
- [39] S. Bai, P. Da, C. Li, Z. Wang, Z. Yuan, F. Fu, M. Kawecki, X. Liu, N. Sakai, J. T.-W. Wang, S. Huettner, S. Buecheler, M. Fahlman, F. Gao, H. J. Snaith, *Nature* **2019**, *571*, 245.
- [40] S. Wang, B. Yang, J. Han, Z. He, T. Li, Q. Cao, J. Yang, J. Suo, X. Li, Z. Liu, S. Liu, C. Tang, A. Hagfeldt, *Energy Environ. Sci.* **2020**, *13*, 5068.
- [41] H. Li, J. Shi, J. Deng, Z. Chen, Y. Li, W. Zhao, J. Wu, H. Wu, Y. Luo, D. Li, Q. Meng, *Adv. Mater.* **2020**, *32*, 1907396.
- [42] M. Abdi-Jalebi, Z. Andaji-Garmaroudi, S. Cacovich, C. Stavarakas, B. Philippe, J. M. Richter, M. Alsari, E. P. Booker, E. M. Hutter, A. J. Pearson, S. Lilliu, T. J. Savenije, H. Rensmo, G. Divitini, C. Ducati, R. H. Friend, S. D. Stranks, *Nature* **2018**, *555*, 497.
- [43] S. Akin, N. Arora, S. M. Zakeeruddin, M. Grätzel, R. H. Friend, M. I. Dar, *Adv. Energy Mater.* **2020**, *10*, 1903090.
- [44] Y. Wang, Q. Liao, J. Chen, W. Huang, X. Zhuang, Y. Tang, B. Li, X. Yao, X. Feng, X. Zhang, M. Su, Z. He, Z. He, T. J. Marks, A. Facchetti, X. Guo, *J. Am. Chem. Soc.* **2020**, *142*, 16632.
- [45] Y. Cho, A. M. Soufiani, J. S. Yun, J. Kim, D. S. Lee, J. Seidel, X. Deng, M. A. Green, S. Huang, A. W. Y. Ho-Baillie, *Adv. Energy Mater.* **2018**, *8*, 1703392.
- [46] B. Yang, J. Suo, E. Mosconi, D. Ricciarelli, W. Tress, F. De Angelis, H.-S. Kim, A. Hagfeldt, *ACS Energy Lett.* **2020**, *5*, 3159.
- [47] M. Salado, R. K. Kokal, L. Calio, S. Kazim, M. Deepa, S. Ahmad, *Phys. Chem. Chem. Phys.* **2017**, *19*, 22905.
- [48] T. A. S. Doherty, A. J. Winchester, S. Macpherson, D. N. Johnstone, V. Pareek, E. M. Tennyson, S. Kosar, F. U. Kosasih, M. Anaya, M. Abdi-Jalebi, Z. Andaji-Garmaroudi, E. L. Wong, J. Madéo, Y.-H. Chiang, J.-S. Park, Y.-K. Jung, C. E. Petoukhoff, G. Divitini, M. K. L. Man, C. Ducati, A. Walsh, P. A. Midgley, K. M. Dani, S. D. Stranks, *Nature* **2020**, *580*, 360.
- [49] Y. Xiang, Z. Ma, X. Peng, X. Li, B. Chen, Y. Huang, *J. Phys. Chem. C* **2020**, *124*, 20765.
- [50] L. Liang, H. Luo, J. Hu, H. Li, P. Gao, *Adv. Energy Mater.* **2020**, *10*, 2000197.
- [51] J. R. Harwell, T. K. Baikie, I. D. Baikie, J. L. Payne, C. Ni, J. T. S. Irvine, G. A. Turnbull, I. D. W. Samuel, *Phys. Chem. Chem. Phys.* **2016**, *18*, 19738.
- [52] C. Chen, Z. Song, C. Xiao, D. Zhao, N. Shrestha, C. Li, G. Yang, F. Yao, X. Zheng, R. J. Ellingson, C.-S. Jiang, M. Al-Jassim, K. Zhu, G. Fang, Y. Yan, *Nano Energy* **2019**, *61*, 141.
- [53] C.-C. Zhang, Z.-K. Wang, S. Yuan, R. Wang, M. Li, M. F. Jimoh, L.-S. Liao, Y. Yang, *Adv. Mater.* **2019**, *31*, 1902222.
- [54] D. Yang, X. Zhou, R. Yang, Z. Yang, W. Yu, X. Wang, C. Li, S. Liu, R. P. H. Chang, *Energy Environ. Sci.* **2016**, *9*, 3071.
- [55] W. Tress, M. Yavari, K. Domanski, P. Yadav, B. Niesen, J.-P. Correa-Baena, A. Hagfeldt, M. Grätzel, *Energy Environ. Sci.* **2018**, *11*, 151.